University Medical School), Takashi Wada (Kanazawa University Graduate School), Kunihiro Yamagata (University of Tsukuba Graduate School), and Shuichi Tsuruoka (Nippon Medical School).

Compliance with ethical standards

Conflict of interest None of authors have any conflicts of interest to disclose for this paper.

References

1. Sugiyama H, Yokoyama H, Sato H, Saito T, Kohda Y, Nishi S, Tsuruya K, Kiyomoto H, Iida H, Sasaki T, Higuchi M, Hattori M, Oka K, Kagami S, Nagata M, Kawamura T, Honda M, Fukasawa Y, Fukatsu A, Morozumi K, Yoshikawa N, Yuzawa Y, Matsuo S, Kiyohara Y, Joh K, Taguchi T, Makino H, Committee for Standardization of Renal Pathological Diagnosis and Working Group for Renal Biopsy Database, Japanese Society of Nephrology. Japan renal biopsy registry: the first nationwide, web-based, and prospective registry system of renal biopsies in Japan. Clin Exp Nephrol. 2011;15:493–503.
2. Sugiyama H, Yokoyama H, Sato H, Saito T, Kohda Y, Nishi S, Tsuruya K, Kiyomoto H, Iida H, Sasaki T, Higuchi M, Hattori M, Oka K, Kagami S, Kawamura T, Takeda T, Hataya H, Fukasawa Y, Fukatsu A, Morozumi K, Yoshikawa N, Shimizu A, Kitamura H, Yuzawa Y, Matsuo S, Kiyohara Y, Joh K, Nagata M, Taguchi T, Makino H, Committee for Standardization of Renal Pathological Diagnosis; Committee for Kidney Disease Registry; Japanese Society of Nephrology. Japan renal biopsy registry and Japan kidney disease registry: committee report for 2009 and 2010. Clin Exp Nephrol. 2013;17:155–73.
3. Yokoyama H, Taguchi T, Sugiyama H, Sato H, Committee for the Standardization of Renal Pathological Diagnosis and for Renal Biopsy and Disease Registry in the Japanese Society of Nephrology. Membranous nephropathy in Japan: analysis of the Japan renal biopsy registry (J-RBR). Clin Exp Nephrol. 2012;16:557–63.
4. Yokoyama H, Sugiyama H, Sato H, Taguchi T, Nagata M, Matsuo S, Makino H, Watanabe T, Saito T, Kiyohara Y, Nishi S, Iida H, Morozumi K, Fukatsu A, Sasaki T, Tsuruya K, Kohda Y, Higuchi M, Kiyomoto H, Goto S, Hattori M, Hataya H, Kagami S, Yoshikawa N, Fukasawa Y, Ueda Y, Kitamura H, Shimizu A, Oka K, Nakagawa N, Ito T, Uchida S, Furuichi K, Nakaya I, Umemura S, Hiromura K, Yoshimura M, Hirawa N, Shigematsu T, Fukagawa M, Hiramatsu M, Terada Y, Uemura O, Kawata T, Matsunaga A, Kuroki A, Mori Y, Mitsuiki K, Yoshida H, Committee for the Standardization of Renal Pathological Diagnosis and for Renal Biopsy and Disease Registry of the Japanese Society of Nephrology, and the Progressive Renal Disease Research of the Ministry of Health, Labour and Welfare of Japan. Renal disease in the elderly and the very elderly Japanese: analysis of the Japan renal biopsy registry (J-RBR). Clin Exp Nephrol. 2012;16:903–20.
5. Furuichi K, Shimizu M, Toyama T, Koya D, Koshino Y, Abe H, Mori K, Satoh H, Imanishi M, Iwano M, Yamauchi H, Kusano E, Fujimoto S, Suzuki Y, Okuda S, Kitagawa K, Iwata Y, Kaneko S, Nishi S, Yokoyama H, Ueda Y, Haneda M, Makino H, Wada T, Research Group of Diabetic Nephropathy, Ministry of Health, Labour, and Welfare of Japan. Japan diabetic nephropathy cohort study: study design, methods, and implementation. Clin Exp Nephrol. 2013;17:819–26.
6. Yonekura Y, Goto S, Sugiyama H, Kitamura H, Yokoyama H, Nishi S. The influences of larger physical constitutions including obesity on the amount of urine protein excretion in primary glomerulonephritis: research of the Japan Renal Biopsy Registry. Clin Exp Nephrol. 2015;19:359–70.
7. Yokoyama H, Sugiyama H, Narita I, Saito T, Yamagata K, Nishio S, Fujimoto S, Mori N, Yuzawa Y, Okuda S, Maruyama S, Sato H, Ueda Y, Makino H, Matsuo S. Outcomes of primary nephrotic syndrome in elderly Japanese: retrospective analysis of the Japan Renal Biopsy Registry (J-RBR). Clin Exp Nephrol. 2015;19:496–505.
8. Mehta RL, Pascual MT, Soroko S, Savage BR, Himmelfarb J, Ikizler TA, Paganini EP. Chertow GM;. Spectrum of acute renal failure in the intensive care unit: the PICARD experience. Kidney Int. 2004;66:1613–21.
9. Mehta RL, Awdishu L, Davenport A, Murray PT, Macedo E, Cerda J, Chakaravarthi R, Holden AL, Goldstein SL. Phenotype standardization for drug-induced kidney disease. Kidney Int. 2015;88:226–34.
10. Churg J, Bernstein J, Glassock RJ, editors. Renal disease, classification and atlas of glomerular disease. 2nd ed. Igaku-Shoin: Tokyo; 1995.
11. Matsuo S, Imai E, Horio M, Yasuda Y, Tomita K, Nitta K, Yamagata K, Tomino Y, Yokoyama H, Hishida A. Revised equations for estimated GFR from serum creatinine in Japan. Am J Kidney Dis. 2009;53:982–92.
12. Kidney Disease: Improving Global Outcomes (KDIGO) Work Group. KDIGO clinical practice guideline for the evaluation and management of Chronic Kidney Disease. Kidney Int Suppl. 2012;2013(3):S1–150.
13. Aithal GP, Watkins PB, Andrade RJ, et al. Case definition and phenotype standardization in drug-induced liver injury. Clin Pharmacol Ther. 2011;89:806–15.
14. Reports of 2007 to 2009 from the study group for Renal Disease Research by a Grant-in-Aid of the Japanese Ministry of Welfare and Labor, 2012. p. 24–25. https://mhlw-grants.niph.go.jp/niph/search/NIDD00.do?resrchNum=201121002A. Accessed 11 Nov 2015(**in Japanese**).
15. Linton AL, Clark WF, Driedger AA, Turnbull DI, Lindsay RM. Acute interstitial nephritis due to drugs: review of the literature with a report of nine cases. Ann Int Med. 1980;93:735–41.
16. Rosen S, Brezis M, Stillman I. The pathology of nephrotoxic injury: a reappraisal. Min Electrol Metab. 1994;20:174–80.
17. Barri YM, Munshi NC, Sukumalchantra S, Abulezz SR, Bonsib SM, Wallach J, Walker PD. Podocyte injury associated glomerulopathies induced by pamidronate. Kidney Int. 2004;65:634–41.
18. Eremina V, Jefferson JA, Kowalewska J, Hochster H, Haas M, Weisstuch J, Richardson C, Kopp JB, Kabir MG, Backx PH, Gerber HP, Ferrara N, Barisoni L, Alpers CE, Quaggin SE. VEGF inhibition and renal thrombotic microangiopathy. N Engl J Med. 2008;358:1129–36.
19. Radhakrishnan J, Perazella MA. Drug-induced glomerular disease: attention required! Clin J Am Soc Nephrol. 2015;10:1287–90.
20. Markowitz GS, Bomback AS, Perazella MA. Drug-induced glomerular disease: direct cellular injury. Clin J Am Soc Nephrol. 2015;10:1291–9.
21. Arend LJ, Nadasdy T. Emerging therapy-related kidney disease. Arch Pathol Labo Med. 2009;133:268–78.

22. Yoshida A, Morozumi K, Suganuma T, Sugito K, Ikeda M, Oikawa T, Fujinami T, Takeda A, Koyama K. Clinicopathological findings of bucillamine-induced nephrotic syndrome in patients with rheumatoid arthritis. Am J Nephrol. 1991;11:284–8.
23. Ohtani H, Wakui H, Komatsuda A, Okuyama S, Masai R, Maki N, Kigawa A, Sawada K, Imai H. Distribution of glomerular IgG subclass deposits in malignancy-associated membranous nephropathy. Nephrol Dial Transplant. 2004;19:574–9.
24. Chronopoulos A, Rosner MH, Cruz DN, Ronco C. Acute kidney injury in the elderly: a review. Contrib Nephrol. 2010;165:315–21.
25. Muriithi AK, Leung N, Valeri AM, Cornell LD, Sethi S, Fidler ME, Nasr SH. Clinical characteristics, causes and outcomes of acute interstitial nephritis in the elderly. Kidney Int. 2015;87:458–64.

INTERNAL MEDICINE

□ ORIGINAL ARTICLE □

Ultrastructural Studies of IgG4-related Kidney Disease

Shinichi Nishi[1], Naofumi Imai[2], Kazuhiro Yoshita[2], Yumi Ito[2], Mitsuhiro Ueno[3] and Takako Saeki[4]

Abstract

Objective Ultrastructural studies of IgG4-related kidney disease (IgG4-RKD) characterized by tubulointerstitial nephritis (TIN) are limited in previous reports due to the rarity of the condition. In the present report, we performed ultrastructural examinations and assessed the pathogenesis of this disease.

Patients Clinicopathological studies were conducted in eight patients diagnosed with IgG4-RKD. Routine light, immunofluorescence and electron microscopy examinations and immunohistochemical assessments of IgG4 were performed using renal biopsy samples.

Results Hypocomplementemia, positive anti-nuclear antibodies and eosinophilia were confirmed in more than half of the cases. Electron dense deposits (EDDs) were frequently found in the glomeruli and interstitium. The rate of deposition was 62.5% in both mesangial areas and Bowman's capsule. EDDs were frequently detected on the tubular basement membrane (TBM) (87.5% of patients). The interstitium also contained EDDs on collagen fibers in 87.5% of the cases and on basement membrane-like materials in areas of fibrosis in 37.5% of the cases. The creatinine clearance levels were significantly lower in the patients with the latter pattern. Meanwhile, the rate of immunoglobulin and/or complement deposition on the TBM was observed in less than 37.5% of patients, and these findings were not entirely coincident with the cases of EDDs on the TBM.

Conclusion EDDs are frequently found in the glomeruli and interstitium in patients with IgG4-RKD; however, immunohistological studies do not provide evidence that IgG4-RKD involves TIN with immune complex nephropathy. The presence of interstitial EDDs may be related to the progression of interstitial fibrosis in the setting of IgG4-RKD.

Key words: plasma cell, electron dense deposit, immune complex

(Intern Med 54: 147-153, 2015)
(DOI: 10.2169/internalmedicine.54.2581)

Introduction

Recently much attention has been paid to the development of IgG4-related nephropathy and/or IgG4-related kidney disease (IgG4-RKD) characterized by tubulointerstitial nephritis (TIN), as these conditions present with unique clinical and histological findings. Initially, IgG4-RKD was reported to be an organ complication associated with autoimmune pancreatitis (AIP) (1, 2). Immunological disorders, such as hypocomplementemia, positive anti-nuclear antibodies and hypereosinophilia, are confirmed clinical features in more than half of patients with IgG4-related systemic diseases, including AIP and IgG4-RKD (3, 4). Based on this background, autoimmune and/or allergic disorders are suspected to underlie the pathogenic mechanisms of IgG4-RKD, although the detailed pathogenesis has not yet been clarified.

The Japanese Society of Nephrology (JSN) published diagnostic criteria for IgG4-RKD in 2011 (5). However, data regarding the electron microscopic findings of IgG4-RKD are limited at present. Some patients exhibit electron dense deposits (EDDs) on the glomerular basement membrane (GBM) and tubular basement membrane (TBM) (1, 2, 6, 7).

[1]Division of Nephrology and Kidney Center, Kobe University Graduate School of Medicine, Japan, [2]Divisions of Clinical Nephrology and Rheumatology, Niigata University Graduate School of Medical and Dental Sciences, Japan, [3]Joetsu University of Education, Japan and [4]Department of Internal Medicine, Nagaoka Red Cross Hospital, Japan
Received for publication January 30, 2014; Accepted for publication June 9, 2014
Correspondence to Dr. Shinichi Nishi, snishi@med.kobe-u.ac.jp

Table 1. Clinical and Laboratory Data in the Cases with IgG4 Relalted Nephropathy

(n=8)

	age years old	sex	SBP mmHg	DBP mmHg	Ccr mL/min/1.73m^2	S-Cr mg/dL	UP g/day	organ complication
case 1	68	male	118	68	36.3	1.37	0.1	
case 2	70	male	132	68	58	0.93	0.6	AIP
case 3	75	male	122	70	66.9	1.23	0.3	
case 4	51	male	150	94	11.2	3.97	0.3	
case 5	83	male	112	60	44.4	4.72	0.7	
case 6	69	male	128	68	35.6	2.36	1.3	AIP
case 7	78	male	167	70	11.8	6.17	1.4	
case 8	76	male	146	60	65	1.21	0.2	
mean	71.3		134.4	69.8	41.2	2.74	0.6	
SD	9.6		18.6	10.6	21.8	1.97	0.5	

SBP: systolic blood pressure, DBP: diastolic blood pressure, Ccr: creatinine clearance, Cr: creatinine
AIP: autoimmune pancreatitis

Table 2. Serelogical Data in the Cases with IgG4 Related Nephropathy

(n=8)

	Eos %	IgG4 mg/dL	IgG mg/dL	IgA mg/dL	IgM mg/dL	C3 mg/dL	C4 mg/dL	CH50 U/mL	ANF times or index
case 1	*40	2,295	305	214	48	*41	*2<	*10	*640
case 2	ND	3,496	924	231	108	52	*2<	*12.0	*320
case 3	6	5,380	623	273	87	*41	*2<	*14.1	*100.1
case 4	*24.7	2,325	587	199	82	118	23	32	ND
case 5	0	3,144	1,340	35	79	56	*6	*16	*2,560
case 6	7	4,001	1,860	145	99	55	*2<	*<10	80
case 7	ND	3,935	670	113	74	57	28	27	<40
case 8	* 8	2,820	1,021	220	102	60	28	30	ND
mean	14	3,425	916	179	85	66	26	30	
SD	15	1,025	494	77	19	25	3	2	

Eos: eosinophil, ANF: anti nulear antibody, ND: not done
* indicates abnormal data.

The presence of ultrastructural abnormalities of the glomeruli and interstitium has not been thoroughly evaluated in patients with IgG4-RKD. We herein summarize the pathological findings of the glomeruli and interstitium observed on electron microcopy in eight cases of IgG4-RKD and discuss the pathogenesis of IgG4-RKD.

Materials and Methods

From 1999 to 2013, 6,342 patients underwent renal biopsies at Niigata University Medical and Dental Hospital, Kobe University Hospital and affiliated hospitals. Informed consent for the renal biopsy was provided by all patients prior to the procedure. Among the patients, eight were diagnosed with IgG4-RKD based on light microscopic observations and clinical findings according to the criteria of the JSN (5). Patients with collagen diseases and vasculitis were excluded, and no subjects met the criteria for systemic lupus erythematosus (SLE), Sjögren's syndrome, anti-neutrophil cytoplasmic antibody (ANCA)-related vasculitis, rheumatoid arthritis or sarcoidosis.

Renal tissues were obtained via needle biopsy. All tissues were examined using routine light microscopy, direct immunofluorescence and electron microscopy. For light immunohistochemical staining, formalin-fixed, paraffin-embedded biopsy specimens were cut into 3-μm thick sections and immunostained with mouse monoclonal antibodies against human IgG4 (Zymed Laboratory, San Francisco, USA, or The Binding Site, Birmingham, UK).

Clinical data

All eight patients were men, with an average age of 71.3± 9.6 (mean ± SD) years at the time of the renal biopsy (Table 1). Two cases involved complications of AIP. Renal imaging revealed multiple low density lesions in two cases on CT and diffuse kidney enlargement in six cases on enhanced CT.

The renal function was deteriorated in all patients. The mean creatinine clearance (Ccr) level was 41.2±21.8 mL/min/1.73 m^2 and the mean serum creatinine (S-Cr) level was 2.74±1.97 mg/dL at the time of biopsy. A significant amount of urinary protein, more than 0.2 g/day, was confirmed in six (75.0%) of the eight cases, and three (37.5%) of the eight patients had hypereosinophilia (Table 2). All patients demonstrated elevated serum IgG4 and IgG levels, with mean values of 3,424.5±1,024.8 mg/dL (cut off level

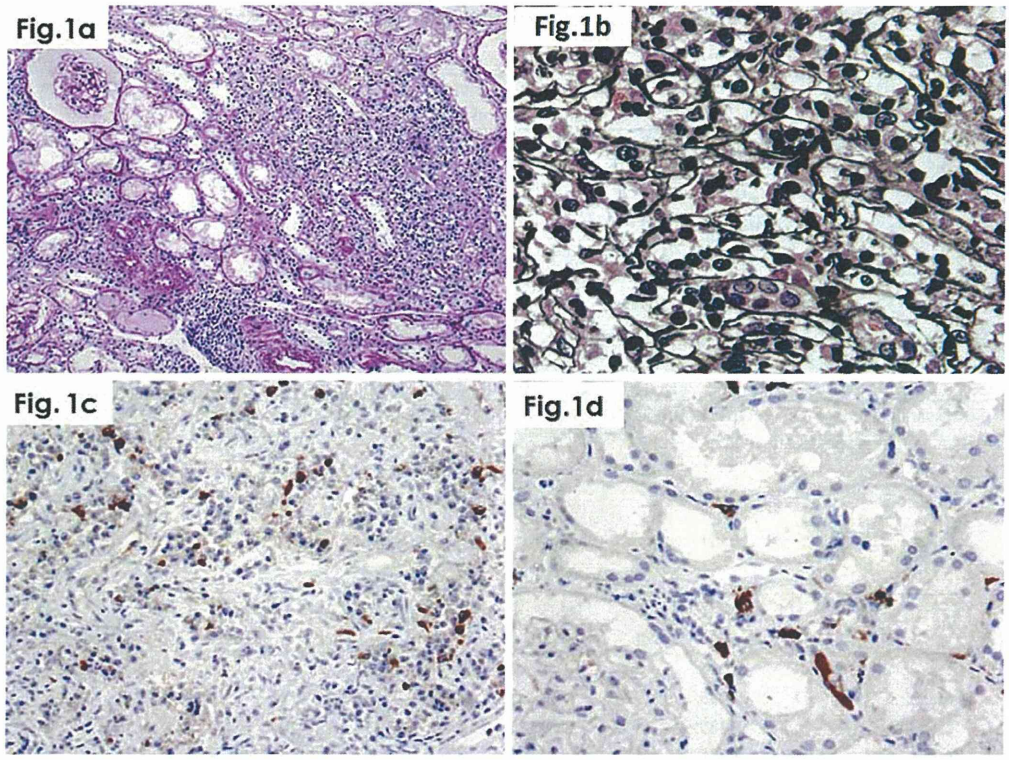

Figure 1. Light microscopy. 1a: Interstitial cell infiltration with a clearly demarcated border between affected and unaffected areas periodic-acid Schiff (PAS) stain ×100. 1b: Specific fibrotic lesions with collagen fibers and infiltrating cells exhibiting storiform fibrosis on periodic acid Silver methenamine (PAM) staining PAM stain ×400. 1c: Immunostaining of paraffin sections with anti-IgG4 antibodies. IgG4-positive plasma cells infiltrating the interstitium in affected areas. 1c: Strong positive findings for IgG4 on the tubular basement membrane (TBM) and interstitium were not confirmed in all cases ×200. 1d: A small amount of IgG4-positive plasma cells was noted in relatively unaffected areas ×400.

<135 mg/dL) and 916.3±494.2 mg/dL, respectively. Hypocomplementemia was noted in five (62.5%) patients, and anti-nuclear antibodies were positive in four (50.0%) patients. No cryoglobulin, M-peak proteins, myeloperoxidase (MPO)-ANCA or proteinase (PR3)-ANCA were detected in any of the patients.

Histological findings

TIN was a dominant histological feature in all cases. The cells comprising areas of massive infiltration primarily included lymphocytes and plasma cells, with occasional eosinophils. The distribution of infiltrating cells exhibited a specific pattern with a well-demarcated border between affected and unaffected areas (Fig. 1a), and the tubular basement membrane displayed thinning in the areas with massive cell infiltration. In the progressive fibrotic lesions, a characteristic 'storiform' pattern of fibrosis was observed surrounding nests of lymphocytes and/or plasma cells on periodic acid-methenamine staining of silver-stained preparations in all cases (Fig. 1b). Almost all glomeruli exhibited minor glomerular abnormalities, excluding two cases of membranous nephropathy.

Immunostaining of paraffin sections with anti-IgG4 antibodies showed infiltration of numerous IgG4-positive plasma cells into the interstitium (Fig. 1c). The number of IgG4-positive plasma cells >10/high power field (HPF) and ratio of IgG4-positive plasma cells/IgG-positive plasma cells exceeded 40% in all cases. Strong positive findings for IgG4 on the TBM and interstitium were confirmed in three (37.5%) of the eight cases. A small amount of IgG4-positive plasma cells was detected in both affected and relatively unaffected areas in the interstitium (Fig. 1d). IgG4 immunostaining also disclosed diffuse reactivity in the glomerular capillary wall in two cases of membranous nephropathy. In the other cases, the glomeruli showed no reaction to anti-IgG4 antibodies. No glomerular deposition of immunoglobulin or complement was observed on routine immunofluorescence examinations, excluding the two cases of membranous nephropathy. C3c deposition along the TBM was noted in three cases and IgG deposition along the TBM was seen in one case (Table 3).

EDDs were detected in various lesions on electron microscopy (Table 4). For example, subepithelial EDDs were observed in four (50.0%) patients, with segmental distribution in two cases and diffuse distribution in the two cases of membranous nephropathy (Fig. 2a) (Table 4). EDD deposi-

Table 3. Immunofluorescet Study in the Cases with IgG4 Related Nephropathy

(n=8)

	findings in light microscopy	glomeruli	Bowman's capsule	TBM
case 1	MGA, TIN	ns	ns	ns
case 2	MGA, TIN	ns	ns	ns
case 3	MGA, TIN	ns	ns	ns
case 4	MGA, TIN	ns	ns	ns
case 5	MGA, TIN	ns	ns	C3c
case 6	MN, TIN	IgG, C3c	C3c, C4	C3c, C4
case 7	MN, TIN	IgG, C3c	ns	IgG, C3c
case 8	MesPGN, TIN	ns	ns	ns

MGA: minor glomerular abnormalities, MN: membranous nephropathy
MesPGN: mesangial proliferative glomerulonephritis
TBM: tubular basement membrane, ns: not specific, ND: not done

Table 4. Electron Microscopic Study in IgG4 Related Nephropathy

(n=8)

	distribution of EDDs						
	subepithelial space	mesangium	subendothelial space	Bowman's capsule	TBM	interstitium on collagen fibers	basement membrane like substances in interstitium
case 1	0	0	0	0	+	+	0
case 2	0	+	0	+	+	0	0
case 3	0	+	0	+	+	+	0
case 4	+	+	0	0	+	+	+
case 5	+	+	0	0	+	+	0
case 6	++	0	0	+	0	+	+
case 7	++	+	+	+	+	+	+
case 8	0	0	0	+	+	+	0
deposition rates	50.0%	62.5%	12.5%	62.5%	87.5%	87.5%	37.5%

tion in mesangial areas was also seen in five (62.5%) of the eight cases; the mesangial EDDs were found in a scattered distribution in small amounts (Fig. 2b). Almost all of the EDDs had a homogenous appearance, although one case involved a mixed pattern of high and low electron dense materials (Fig. 2c). In addition, a small amount of subendothelial deposits was noticed in only one (12.5%) case. In contrast, EDD deposition in Bowman's capsules was detected in five (62.5%) of the eight cases (Fig. 2d), and a portion of the plasma cells contained a well-developed rough endoplasmic reticulum (Fig. 3a). Lymphocytes and eosinophils also infiltrated the interstitium (Fig. 3b). Furthermore, EDDs were visible on the TBM and collagen fibers themselves in 87.5% of the cases (Fig. 3b, c) and on basement membrane-like substances within fibrotic lesions in 37.5% of the cases (Fig. 3d).

Relationships between the clinical data and the presence of EDDs

There were no clear relationships between the presence of serological disorders, such as hypocomplementemia and positive antinuclear factor (ANF), and the presence of EDDs on Bowman's capsules, the TBM or interstitium. Cases 1 to 4 and 8 involved no deposition of IgG or C3c on the TBM, although these patients exhibited EDDs on the TBM. Three patients with EDDs on basement membrane-like substances within fibrotic interstitial lesions showed significantly lower Ccr levels, less than 36.0 mL/min/1.73 m^2, compared to that observed in the other cases ($p<0.05$; statistically significant difference according to the Wilcoxon test).

Discussion

Previously reported organ disorders associated with IgG4-RKD include AIP as well as Mikulicz's disease (8), sclerosing cholangitis (9) and retroperitoneal fibrosis (10). However, a few patients suffer from IgG4-RKD alone, without other types of organ involvement (3, 11, 12).

The pathological description of IgG4-RKD is limited to the findings of light microscopic and immunohistochemical assessments conducted in previous cross-sectional case studies. For example, Saeki (3), Kawano (13) and Yoshita (14) et al. each evaluated at least 20 patients with IgG4-RKD in their series using histological evaluations of light and immunohistochemical modalities without electron microscopy. To date, observations with electron microscopy have been restricted to limited case reports (1, 2, 6, 7, 15-17). Recently Yamaguchi et al. (18) comprehensively reported the ultrastructural findings of 10 cases. The authors found the deposition of EDDs on the TBM and interstitium in 100% and

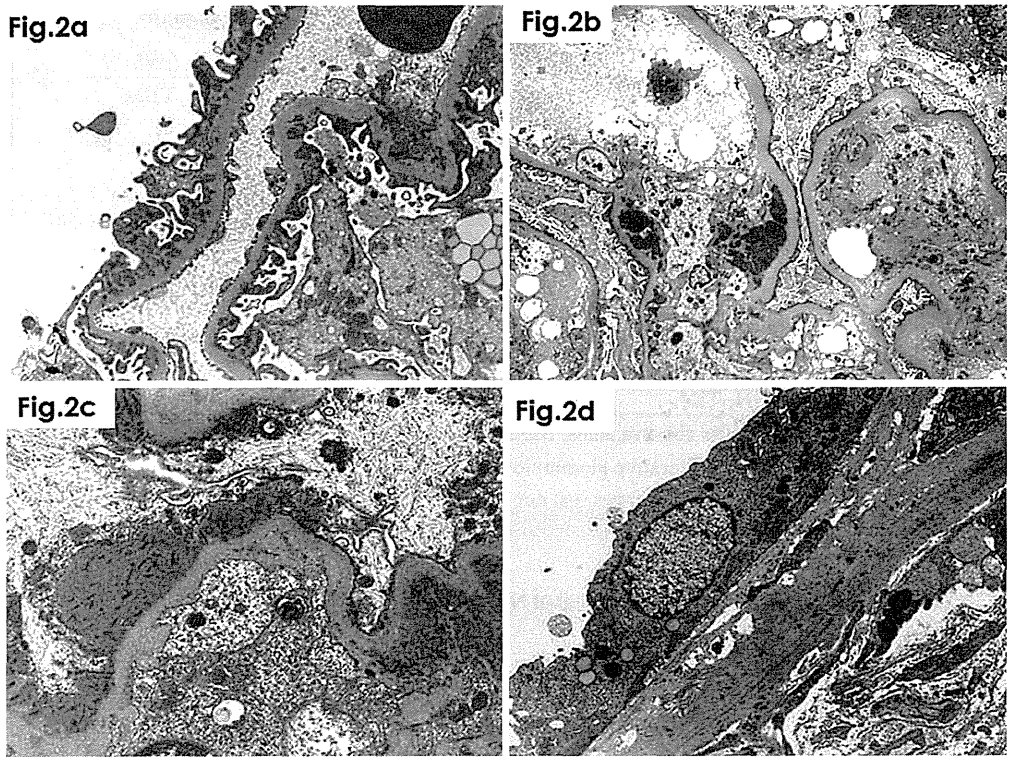

Figure 2. Electron microscopy of the glomeruli. 2a: Subepithelial deposits exhibiting a segmental distribution. 2b: Mesangial deposits in paramesangial lesions. 2c: EDDs showing a mixed pattern of high and low electron dense materials. 2d: EDDs on Bowman's capsules ×3,500.

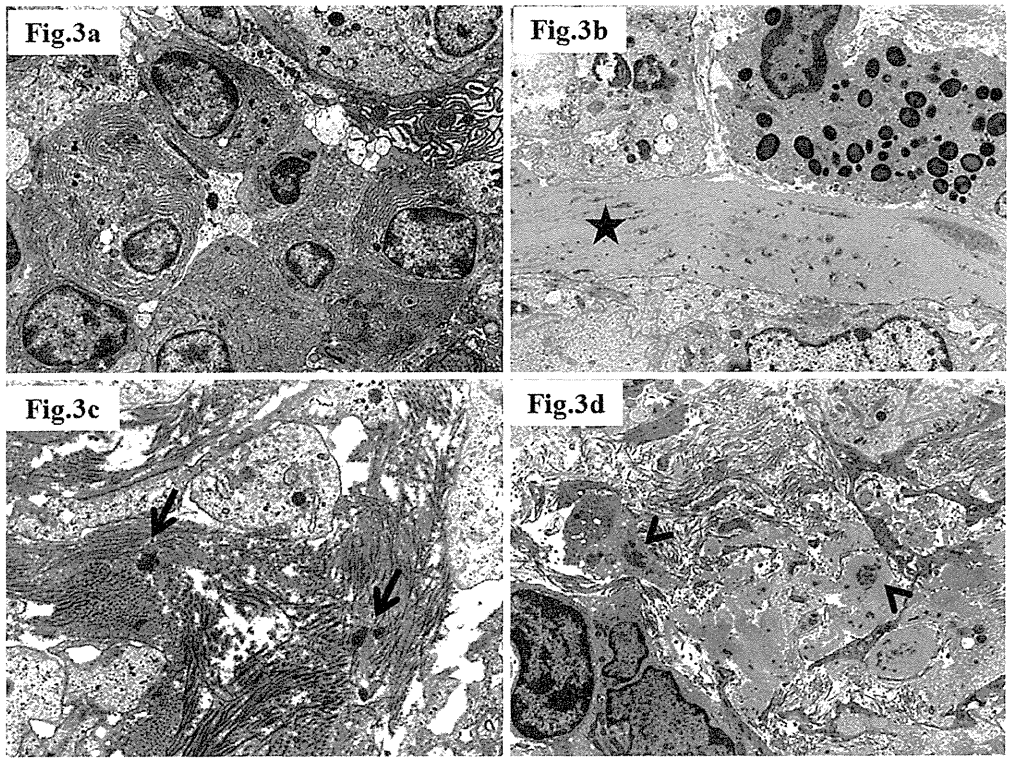

Figure 3. Electron microscopy of the interstitium. 3a: Some plasma cells showed a tendency to assemble together. A well-developed rough endoplasmic reticulum was often observed ×3,500. 3b: EDDs on the TBM (star) and eosinophils in the interstitium (right upper cell) ×5,000. 3c: EDDs on collagen fibers (arrows) ×8,000. 3d: EDDs on basement membrane like-substances in the interstitium (arrowheads) ×8,000.

70% of cases, respectively. Meanwhile, Raissian et al. (19) documented the presence of EDDs on the TBM in 92.6% cases of IgG4-RKD. In the present study, the rate of EDD deposition was 87.5% on both the TBM and interstitium. Furthermore, we noticed two types of deposition in the interstitium: the presence of EDDs on collagen fibers themselves (87.5%) and the presence of EDDs on basement membrane-like materials within fibrotic lesions (37.5%). Based on our experience, interstitial EDDs are seldom observed in other types of TIN, including cases of TIN induced by drugs or collagen diseases. The EDDs observed in patients with IgG4-RKD may therefore have affinity for the extracellular matrix of the basement membrane, as EDDs are frequently observed on the GBM (7, 18), Bowman's capsule and TBM (1, 6, 7, 15, 18).

Cornell et al. (7) previously reported the existence of subepithelial EDDs in two of eight cases. Among our eight patients, four (50.0%) had subepithelial deposits, including two patients with membranous nephropathy and one patient with subendothelial EDDs along the GBM. In the present study, EDDs were also found to be deposited on Bowman's capsule and the TBM at higher rates, 62.5% and 87.5%, respectively, similar to that reported by Yamaguchi (18).

The immunopathogenic role of EDDs deposited on the TBM has not been fully clarified. The deposition of EDDs on the TBM is suspected to represent an immunopathological insult leading to the development of interstitial lesions in patients with lupus nephritis (20) and autoimmune TIN associated with anti-TBM antibodies (21). Additionally, EDDs are often detected on the TBM on kidney graft biopsies in patients without rejection (22, 23).

It should be carefully determined whether IgG4-RKD is an immune complex type of nephropathy. The immunofluorescence studies performed in the present series showed deposition of C3c or IgG on the TBM in only three (28.6%) cases, whereas most of the patients had EDDs on the TBM. In contrast, the immunohistochemical studies with anti-IgG4 antibodies did not show any remarkable reactions on the TBM on light microscopy. Similar results have been documented in previous articles (2, 4, 6, 11). These observations suggest that EDDs are not necessarily immune complexes involving IgG4. Subclass molecules of IgG exhibit distinct characteristics during immunological reactions. For example, it has been proven that IgG4 molecules do not have the ability to activate the complement cascade (24, 25). Detlefsen et al. (26) demonstrated the positive deposition of C3c, IgG4 and IgG on the basement membrane of the pancreatic duct in patients with AIP using immunofluorescence. The authors suspected that immune complex formation on the basement membrane triggered tissue destruction in cases of AIP. The pathological significance and structural components of EDDS remain unclear. Therefore, it is necessary to follow patients with renal involvement of IgG4-RKD by monitoring for immunoglobulin, complement and/or EDD deposition on the TBM and interstitium. In particular, in the present study, EDDs were found on basement membrane-like substances in fibrotic lesions in the patients with a significantly reduced renal function ($p<0.05$). This finding suggests the presence of a specific pathological process involving interstitial sclerotic changes in patients with IgG4-RKD. The clinical course of IgG4-RKD is usually responsive to steroids, although some patients exhibit deterioration of the renal function under steroid therapy (27).

In conclusion, we found that IgG4-RKD frequently presents with deposition of EDDs in multiple areas, including the glomeruli and interstitium. In particular, two types of EDD deposition in the renal interstitium were found in the present study: deposition on collagen fiber themselves and that on basement membrane-like substances in fibrotic lesions. However, our clinicopathological data did not demonstrate that EDD formation results from immune complex activation. Further investigation is therefore necessary in order to clarify the pathogenesis of IgG4-RKD in terms of both immunological and pathological perspectives.

Author's disclosure of potential Conflicts of Interest (COI).
Shinichi Nishi: Honoraria, Chyugai Seiyaku, Kyowa Hakko Kirin and Novartis Pharma.

Financial Support
This study was supported in part by a Grant-in-Aid for Progressive Renal Disease Research, Research on Rare and Intractable Diseases and Research on Amyloidosis from the Ministry Labour and Welfare of Japan and a Grant-in-Aid issue number 24591199 from the Ministry of Education.

References

1. Takeda S, Haratake J, Kasai T, et al. IgG4-associated idiopathic tubulointerstitial nephritis complicating autoimmune pancreatitis. Nephrol Dial Transplant **19**: 474-476, 2004.
2. Uchiyama-Tanaka Y, Mori Y, Kimura T, et al. Acute tubulointerstitial nephritis associated with autoimmune-related pancreatitis. Am J Kidney Dis **43**: e18-e25, 2004.
3. Saeki T, Nishi S, Imai N, et al. Clinicopathological characteristics of patients with IgG4-related tubulointerstitial nephritis. Kidney Int **78**: 1016-1023, 2010.
4. Nishi S, Imai N, Yoshida K, et al. Clinicopathological findings of immunoglobulin G4-related kidney disease. Clin Exp Nephrol **15**: 810-819, 2011.
5. Kawano M, Saeki T, Nakashima H, et al. Proposal for diagnostic criteria for IgG4-related kidney disease. Clin Exp Nephrol **15**: 615-626, 2011.
6. Watson SJ, Jenkins DA, Bellamy CO. Nephropathy in IgG4-related systemic disease. Am J Surg Pathol **30**: 1472-1477, 2006.
7. Cornell LD, Chicano SL, Deshpande V, et al. Pseudotumors due to IgG4 immune-complex tubulointerstitial nephritis associated with autoimmune pancreatocentric disease. Am J Surg Pathol **31**: 1586-1597, 2007.
8. Yamamoto M, Harada S, Ohara M, et al. Clinical and pathological differences between Mikulicz's disease and Sjögren's syndrome. Rheumatology **44**: 227-234, 2005.
9. Deshpande V, Sainani NI, Chung RT, et al. IgG4-associated cholangitis: a comparative histological and immunophenotypic study with primary sclerosing cholangitis on liver biopsy material. Mod Pathol **22**: 1287-1295, 2009.
10. Zen Y, Onodera M, Inoue D, et al. Retroperitoneal fibrosis: a

clinicopathologic study with respect to immunoglobulin G4. Am J Surg Pathol **33**: 1833-1839, 2009.

11. Saeki T, Saito A, Yamazaki H, et al. Tubulointerstitial nephritis associated with IgG4-related systemic disease. Clin Exp Nephrol **11**: 168-173, 2007.

12. Saeki T, Nishi S, Ito T, et al. Renal lesions in IgG4-related systemic disease. Intern Med **46**: 1365-1371, 2007.

13. Kawano M, Mizushima I, Yamaguchi Y, et al. Immunohistochemical characteristics of IgG4-related tubulointerstitial nephritis: detailed analysis of 20 Japanese cases. Int J Rheumatol **2012**: 609795, 2012.

14. Yoshita K, Kawano M, Mizushima I, et al. Light-microscopic characteristics of IgG4-related tubulointerstitial nephritis: distinction from non-IgG4-related tubulointerstitial nephritis. Nephrol Dial Transplant **27**: 2755-2761, 2012.

15. Saeki T, Imai N, Ito T, et al. Membranous nephropathy associated with IgG4-related systemic disease and without autoimmune pancreatitis. Clin Nephrol **71**: 173-178, 2009.

16. Tsubata Y, Akiyama F, Oya T, et al. IgG4-related chronic tubulointerstitial nephritis without autoimmune pancreatitis and the time course of renal function. Intern Med **49**: 1593-1598, 2010.

17. Mori Y, Kishimoto N, Yamahara H, et al. Predominant tubulointerstitial nephritis in a patient with systemic lupus nephritis. Clin Exp Nephrol **9**: 79-84, 2005.

18. Yamaguchi Y, Kanetsuna Y, Honda K, et al. Characteristic tubulointerstitial nephritis in IgG4-related disease. Japanese study group on IgG4-related nephropathy. Hum Pathol **43**: 536-549, 2012.

19. Raissian Y, Nasr SH, Larsen CP, et al. Diagnosis of IgG4-related tubulointerstitial nephritis. J Am Soc Nephrol **22**: 1343-1352, 2011.

20. Mori Y, Kishimoto N, Yamahara H, et al. Predominant tubulointerstitial nephritis in a patient with systemic lupus nephritis. Clin Exp Nephrol **9**: 79-84, 2005.

21. Orfila C, Vega-Vidallé C, Suc JM. Ultrastructural changes of tubular basement membranes in immunologic renal tubular lesions in humans. Ultrastruct Pathol **14**: 121-128, 1990.

22. Shiozawa S, Ichikawa T, Nakazawa K, Ehara T, Shigematsu H. A case of an ABO-incompatible renal transplant with abundant intratubular basement membrane immune deposits. Clin Transplant **16** (Suppl 8): 68-71, 2002.

23. Orfila C, Durand D, Vega-Vidallé C, Suc JM. Immunofluorescent deposits on the tubular basement membrane in human renal transplant. Nephron **57**: 149-155, 1991.

24. Aalberse RC, Dieges PH, Knul-Bretlova V, et al. IgG4 as a blocking antibody. Clin Rev Allergy **1**: 289-302, 1983.

25. Aalberse RC, van der Gaag R, van Leeuwen J. Serologic aspects of IgG4 antibodies. I. Prolonged immunization results in an IgG4-restricted response. J Immunol **130**: 722-726, 1983.

26. Detlefsen S, Bräsen JH, Zamboni G, Capelli P, Klöppel G. Deposition of complement C3c, immunoglobulin (Ig)G4 and IgG at the basement membrane of pancreatic ducts and acini in autoimmune pancreatitis. Histopathology **57**: 825-835, 2010.

27. Saeki T, Kawano M. IgG4-related kidney disease. Kidney Int **85**: 251-257, 2014.

Pathology International

Pathology International 2015; **65**: 374–378 doi:10.1111/pin.12302

Short Communication

Hypoelectrolytic isoosmotic solution for infusion prevents saline-induced ultrastuructural artifacts of renal biopsy specimens

Yasuhiro Nakamura,[1] Keely M. McNamara,[1] Shin Onodera,[2] Yasunori Kitamoto,[3] Kiyomi Kisu,[4] Yukiko Shibahara,[1] Akira Kurosu,[5] Hironobu Sasano,[1] Hiroshi Sato[4,6] and Kensuke Joh[1]

[1]Department of Pathology, [4]Division of Nephrology, Endocrinology and Vascular medicine, Graduate School of Medicine, [6]Clinical Pharmacology and Therapeutics, Graduate School of Pharmaceutical Sciences, Tohoku University, Departments of [2]Pathology, [3]Laboratory Medicine, Japan Community Health Care Organization Sendai Hospital, Sendai and [5]Department of Legal Medicine, Dokkyo Medical University, Shimotsuga, Japan

Artifacts in the process of specimen preparation are frequent in ultrastructural evaluation of renal biopsy. We hypothesized that the common practice of wrapping kidney biopsy specimens in saline-soaked gauze to prevent the drying of the specimens could be the major factor of artifacts. In this study, whole kidneys from two male Sprague-Dawley rats were used. Before fixation, fresh small cubes of kidney tissue were macerated in saline (Saline group) or hypoelectrolytic isoosmotic solution for infusion (HISI group) (Sorita T3 or SOLDEM 3A) for 10 or 30 min. Then, the specimens were processed by 1% OsO_4 in 0.1 M phosphate buffer (pH 7.4) and embedded by *EPON 812* for ultramicroscopic analysis. In the Saline group, ultrastructural examination revealed swollen podocyte, swollen capillary protuberance of the mesangium into the glomerular capillary loop, tubular cells with swollen mitochondria and microvilli, and the smooth muscle cells in the arteriolar wall with marked vacuolar degeneration were detected after 10 min maceration in saline and these findings become more pronounced after 30 min maceration. However, in the HISI group, these artifacts were not identified or limited within 30 min. It is postulated that HISI solution could prevent the artifacts, and be used for soaking and wrapping instead of physiologic saline solution.

Key words: artifacts, electron micrograph, physiologic saline, renal biopsy

Ultrastructural examination is still pivotal in the diagnosis of renal biopsies despite the recent development of immunohistochemistry or molecular analyses.[1] However, artifacts on the electron micrograph of renal biopsy are quite common. This can be caused by multiple factors, especially the drying out of the specimens because of the time lapse between removal and effective fixation, and mechanical damage including osmolality, pH and embedding.[2–4] These artifacts disturb detailed observations and result in misdiagnosis. Introduction of such artifacts may be particularly problematic when small specimens of renal biopsies are maintained on saline soaked gauze in order to prevent drying of the specimens prior to dividing the specimens into multiple pieces for light microscopic observation, immunofluorescence analysis and ultrastructural observation. This treatment has been done in order to avoid the most serious and deleterious artifacts, i.e., drying of the specimens. Therefore, in this study, we aimed to address whether saline soaked gauze is a potential cause of artifacts in ultrastructural analysis and if other approaches, such as the substitution of an alternate buffer, may prevent damage and thus lead to an improvement in electron micrograph clarity, which could subsequently result in the more accurate interpretation of the ultrastructural findings in renal biopsy specimens.

MATERIALS AND METHODS

Kidney tissues from two male Sprague-Dawley (SD) rats (8 weeks) were used in this study. Each rat was killed with deep anesthesia. Before fixation (2.5% glutaraldehyde + 2% paraformaldehyde in 0.1 M phosphate buffer), fresh small cubes of the tissue were macerated in either isotonic physiologic saline (NaCl; 9 g/L, Na^+ 154 mEq/L, Cl^- 164 mEq/L,

Correspondence: Yasuhiro Nakamura, MD, PhD, Department of Pathology, Tohoku University School of Medicine, 2-1 Seiryo-machi, Aoba-ku, Sendai 980-8575, Japan. Email: yasu-naka@patholo2.med.tohoku.ac.jp

Received 8 June 2014. Accepted for publication 28 March 2015.

285 mosm) for 10 min or 30 min (Saline group), or in a hypoelectrolytic iso-osmotic solution for infusion (HISI group) (Sorita T3 (Ajinomoto Pharmaceuticals, Tokyo, Japan) containing NaCl 0.9 g, KCl 1.49 g, L-sodium lactate $C_3H_5NaO_3$ 2.24 g, and glucose 43 g per 1 liter dest. water, pH 3.5–6.5, Na^+ 35 mEq/L, K^+ 20 mEq/L, Cl^- 35 mEq/L, L-Lactate 20 mEq/L, 285 mosm or SOLDEM 3A (Terumo Co., Tokyo, Japan) containing NaCl 0.9 g, KCl 1.49 g, L-sodium lactate $C_3H_5NaO_3$ 2.24 g, and glucose 43 g per 1 liter dest. water, pH 5.0–6.5, Na^+ 35 mEq/L, K^+ 20 mEq/L, Cl^- 35 mEq/L, L-Lactate 20 mEq/L, 285 mosm) for 10 min and 30 min. In the Control group, the tissues were dropped directly into the fixative (Control group). After the fixation, the samples were processed by 1% OsO4 in 0.1 M phosphate buffer (pH 7.4) and embedded for observation. Each group was composed of five pieces of kidney tissue, respectively. For morphological analysis, the following parameters were evaluated: the size of the capillary lumen (capillary), the thickness of lamina densa (capillary), the thickness of foot process around pores (endothelium), the larger diameter (endothelium), the width of foot process (podocyte), the size (podocyte), the width of mitochondria (podocyte), the width of capillary protuberance (mesangium), the width of peroxisome (proximal tubules), the width of mitochondria (proximal tubules), the width of microvilli (proximal tubules) and the number of vacuoles (artery). The Ethics Committee of Japan Community Health Care Organization Sendai Hospital (Sendai, Miyagi, Japan) approved this study. Regarding these evaluations, five cells or organelles were analyzed and evaluated in the respective specimens except for the number of vacuoles (artery). The number of vacuoles (artery) was analyzed and evaluated in an artery of the respective specimens.

Statistical analysis

The statistical differences between two groups were evaluated using the unpaired *t*-test. $P < 0.05$ was considered significant.

RESULTS

In the Control group in which fixation was immediately performed, no morphological abnormalities were detected (Figs 1–3). However, electron micrographs of the Saline group exhibited marked artifacts (Figs 1–3). These included swollen podocyte with dilated mitochondria, mesangium with swollen capillary protuberance into the glomerular capillary loop, tubules with swollen mitochondria and microvilli, and the smooth muscle cells of the arteriole with vacuolar degeneration. These artifacts were apparent in the Saline group with 10 min maceration and became more pronounced after 30 min. maceration. The tissues macerated in HISI, however, exhibited no or limited abnormal findings at the 10 or 30 min time points (Figs 1–3). Their electron micrographs were almost identical to those of the Control group (Figs 1–3). The quantification of the artificial changes is summarized in Table 1.

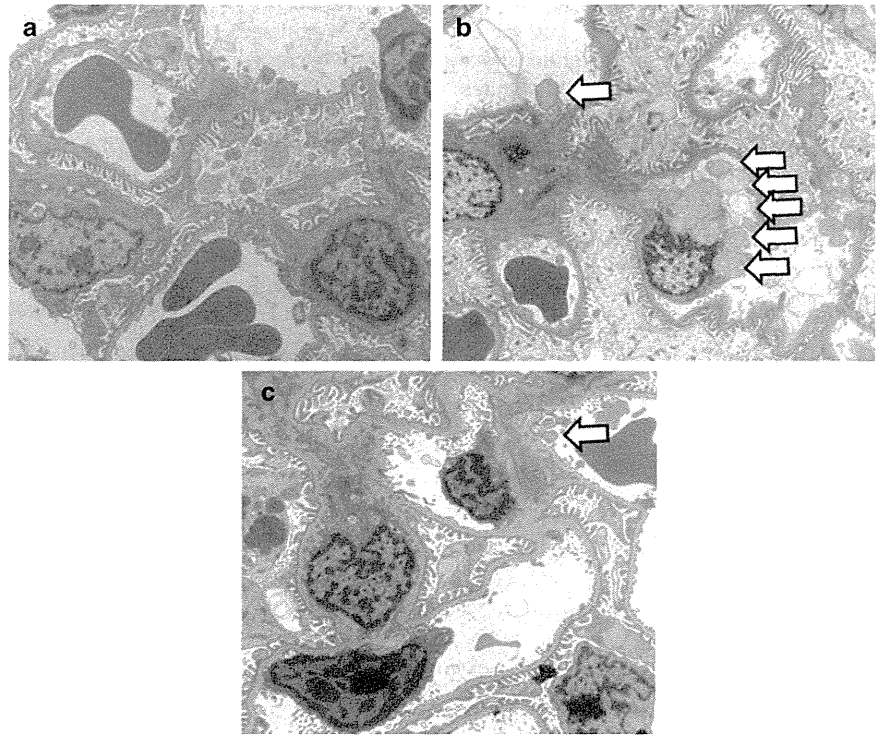

Figure 1 Representative artifacts in the glomerulus. (**a**) No remarkable change was found in the Control group. (**b**) Swollen podocyte and mesangium showing a swollen capillary protuberance into the glomerular capillary loop (white arrow) were found in saline solution (Saline group, 30 min). (**c**) Swollen podocyte and mesangium showing a swollen capillary protuberance into the glomerular capillary loop (white arrow) were focally detectable in HISI infusion solution (Solita-T3) (HISI group, 30 min).

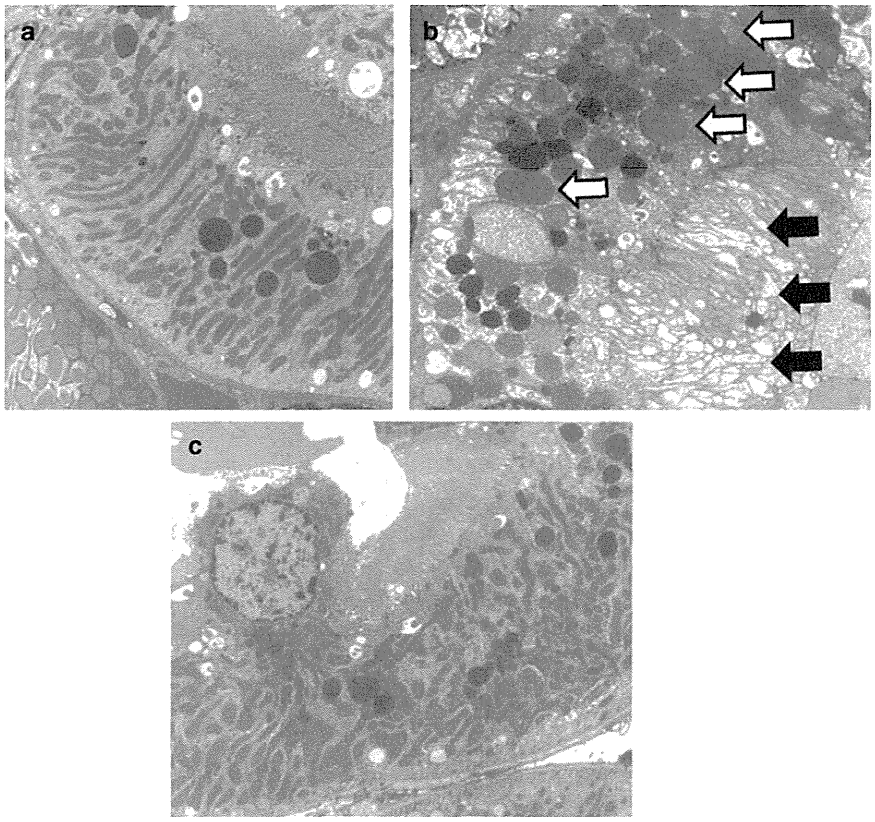

Figure 2 Representative artifacts in the tubulus. (**a**) No remarkable change was found in the Control group. (**b**) Swelling of mitochondria (white arrow) and microvillus (black arrow) was detected in saline solution (Saline group, 30 min). (**c**) No remarkable change was found in the tubulus in HISI infusion solution (Solita-T3) (HISI group, 30 min).

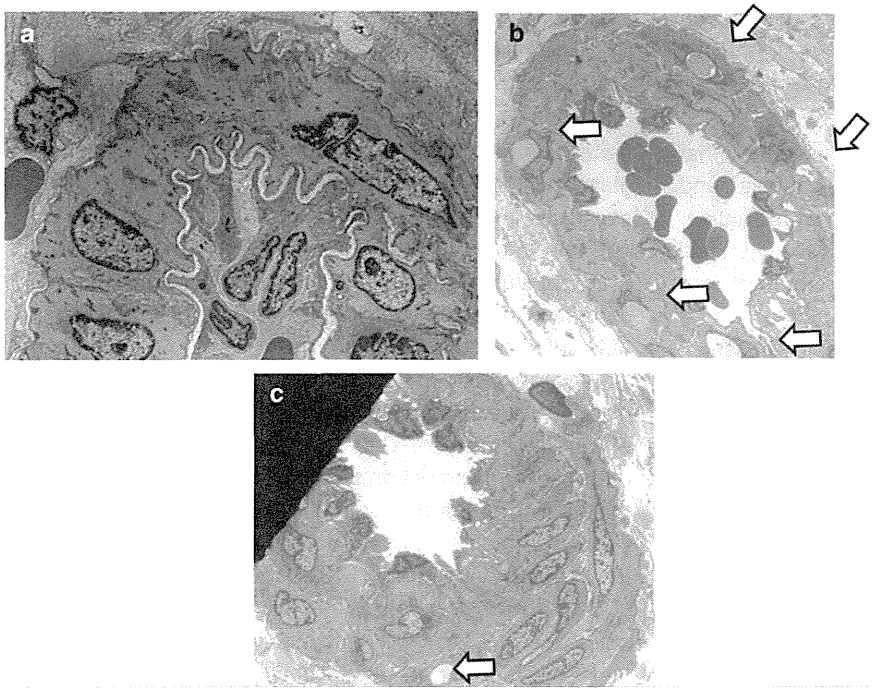

Figure 3 Representative artifacts in the arterioles. (**a**) No remarkable change was found in the Control group. (**b**) Vacuole formation in the arteriolar medial wall was detected in saline solution (Saline group, 10 min) (white arrow). (**c**) The vacuole formation was not remarkable in HISI infusion solution (Solita-T3) (HISI group, 10 min) (white arrow).

DISCUSSION

Practically, the differentiation between the genuine pathological changes and artifacts requires experience. Therefore, any approaches that minimize the introduction of artifacts greatly aid the diagnostic accuracy of renal biopsies. This study aimed to address the possibility that the handling of renal biopsies on physiologic saline-soaked gauze causes

Table 1 The quantification of the artificial changes

		Saline group (1st)		Saline group (2nd)		HISI group (1st)		HISI group (2nd)	
		10 min	30 min	10 min	30 min	Sorita R T3 10 min	30 min	SOLDEM 3 10 min	30 min
Capillary lumen	Size of the capillary lumen (nm)	7794 ± 1947	6783 ± 1076	9043 ± 2435	8551 ± 1589	7714 ± 451	6384 ± 770	9689 ± 1032	9228 ± 1803
	Thickness of lamina densa (nm)	77 ± 5	109 ± 17	77 ± 11	114 ± 18	74 ± 12	106 ± 9	86 ± 18	83 ± 8*
Endothelium	Thickness of foot process around pores (nm)	74 ± 5	75 ± 12	74 ± 7	77 ± 11	90 ± 26	72 ± 7	80 ± 13	80 ± 13
	Larger diameter (nm)	6916 ± 1379	5852 ± 936	4860 ± 2174	6152 ± 1216	6916 ± 1307	6384 ± 758	6090 ± 1466	5321 ± 561
Podocyte	Width of foot process (nm)	399 ± 105	237 ± 29	253 ± 54	262 ± 69	207 ± 45*	213 ± 69	197 ± 30	225 ± 37
	Size (nm)	460180 ± 139365	583870 ± 227387	672875 ± 366205	423104 ± 68351	356440 ± 203972	231420 ± 98792*	110736 ± 61963*	264075 ± 71863*
	Width of mitochondria (nm)	505 ± 197	944 ± 152	372 ± 49	739 ± 247	466 ± 200	439 ± 197*	305 ± 122	375 ± 77*
Mesangium	Width of capillary protuberance (nm)	1702 ± 647	1835 ± 146	1140 ± 258	1078 ± 475	931 ± 133*	705 ± 324*	800 ± 88*	554 ± 199
Proximal tubules	Width of peroxisome (nm)	1410 ± 288	1862 ± 326	1476 ± 175	1384 ± 188	1835 ± 318	1569 ± 510	1015 ± 148*	1261 ± 253
	Width of mitochondria (nm)	1623 ± 288	1623 ± 605	1415 ± 228	1969 ± 296	505 ± 130*	745 ± 152*	892 ± 97*	1154 ± 77*
	Width of microvilli (nm)	231 ± 15	426 ± 36	151 ± 7	354 ± 103	125 ± 7*	120 ± 9*	111 ± 13*	117 ± 18*
Artery	Number of vacuoles (per/artery)	2	5	3	5	1	2	0	2

The data were presented as mean ± standard deviation (SD), except for the number of vacuoles (artery). *indicates statistical significance ($P < 0.05$) compared to the Saline group performed in the same experiment and timepoint.

artifacts in subsequent electron microscopy analysis. In addition, we tested if such artifacts could be prevented by the substitution of a buffer in place of isotonic saline. In order to model this situation, we used kidney tissues from male SD rats soaked in either isotonic saline or HISI and then fixed, compared with electron microscopy images of control tissues fixed immediately following the taking of the kidney tissue by renal biopsy as a gold standard of tissue preparation.

The results of the present study clearly demonstrated that isotonic physiologic saline caused glomerular, tubular and vascular artifacts of renal biopsy specimens prior to fixation. It is entirely true that tissues for electron microscopy should be fixed in glutaraldehyde directly after biopsy, practical considerations such as the use of the one biopsy specimen for multiple diagnostic purposes (i.e. light microscopy for tissue, fluorescent staining and electron microscopy) often dictates that temporary storage on gauze saturated with saline may be required to avoid the specimen drying out before fixation.

In order to reconcile the ideal situation, i.e., immediate fixation after the biopsy with the practical aspects, we sought to evaluate whether alternate and readily available buffers could preserve tissue morphological architectures, thus preventing the introduction of the artifacts detailed above.

While isotonic saline attempts to preserve tissue morphology through the maintenance of a constant concentration of sodium ions inside and outside of the cells, the maintenance of osmotic balance in mammalian cells is, in reality, more complicated than this. In the human body the osmotic balance of the cells is not maintained by passive diffusion, but by active transport of ions over the cell membrane. In the case of sodium, high concentrations of extracellular sodium are maintained against its electrochemical gradient by an ATP-driven sodium potassium pump.[5] This pump links the export of sodium and import of potassium ions from the cell against their respective electrochemical chemical gradients (Na extracellular 145 mM vs. intracellular 5–15 mM; K intracellular 140 mM, extracellular 5 mM).[5] Due to this link between sodium and potassium ions, we hypothesized that a buffer containing potassium and 4.3% glucose could help the maintenance of morphological architecture of the specimens, even after a cessation of sodium and potassium ion pump due to a removal of the tissue from the body.

In this study, we used HISI as it is more complex buffer consisting of sodium ions at one quarter of the concentration of isotonic saline, chloride ions at a similar concentration to isotonic saline, potassium ions and glucose. It is also a commonly available buffer in the operation room where renal biopsy is performed. This solution is, therefore, potentially practical to implement and an inexpensive alternative to isotonic saline in the preparation of renal biopsies. While this study was not designed to address the mechanism behind the better performance of HISI we suggest that the contributions of potassium ions and glucose in the buffer could control cellular osmolality and thus better preserve the cellular architecture for electron microscopy examination.

In conclusion, despite its isotonic nature, even a relatively brief (10 min and 30 min) exposure to saline did introduce artifacts in electron micrographs of renal tissues. On the other hand, HISI prevents this formation of artifacts, possibly due to the presence of potassium salts and glucose. Results

of this study suggest that the replacement of saline with HISI could provide a simple and cost effective method to minimize artifacts associated with tissue preparation of renal biopsy specimens.

ACKNOWLEDGMENT

This study was supported by the Grant in Aid for Scientific Research of Japan Society for the Promotion of Science.

DISCLOSURE

None declared.

REFERENCES

1 Haas M. A reevaluation of routine electron microscopy in the examination of native renal biopsies. *J Am Soc Nephrol* 1997; **8**: 70–76.
2 Olsen TS, Racusen LC, Solez K. Ultrastructural investigation of renal biopsies: A discussion of artifacts and special methodology. *J Electron Microsc Tech* 1988; **9**: 283–91.
3 Osborne CA, Low DG. Size, adequacy, and artifacts of canine renal biopsy samples. *Am J Vet Res* 1971; **32**: 1865–71.
4 Maunsbach AB. The influence of different fixatives and fixation methods on the ultrastructure of rat kidney proximal tubule cells. II. Effects of varying osmolality, ionic strength, buffer system and fixative concentration of glutaraldehyde solutions. *J Ultrastruct Res* 1966; **15**: 283–309.
5 Alberts B, Johnson A, Lewis J, Raff M, Roberts K, Walter P. Chapter 11. Membrane transport of small molecules and the electrical properties of membranes. In: Gibbs S, ed. *Molecular Biology of the Cell*, 4th edn. New York: Garland Science, 2002; 615–29.

Am J Physiol Renal Physiol 308: F487–F499, 2015.
First published December 10, 2014; doi:10.1152/ajprenal.00206.2014.

A functional (pro)renin receptor is expressed in human lymphocytes and monocytes

Kaori Narumi,[1]* Takuo Hirose,[1,2]* Emiko Sato,[1,3] Takefumi Mori,[1,4] Kiyomi Kisu,[1] Mayuko Ishikawa,[1] Kazuhito Totsune,[5,6] Tomonori Ishii,[7] Atsuhiro Ichihara,[8] Genevieve Nguyen,[2] Hiroshi Sato,[1,3] and Sadayoshi Ito[1,4]

[1]*Division of Nephrology, Endocrinology, and Vascular Medicine, Tohoku University Graduate School of Medicine, Sendai, Japan;* [2]*Center for Interdisciplinary Research in Biology (CIRB), College de France, and CNRS UMR 7241 and INSERM U1050, Paris, France;* [3]*Department of Clinical Pharmacology and Therapeutics, Tohoku University Graduate School of Pharmaceutical Science, Sendai, Japan;* [4]*Division of Integrative Renal Replacement Therapy, Tohoku University Graduate School of Medicine, Sendai, Japan;* [5]*Department of Social Welfare, Faculty of Synthetic Welfare, Tohoku Fukushi University, Sendai, Japan;* [6]*Department of Planning for Drug Development and Clinical Evaluation, Tohoku University Graduate School of Pharmaceutical Science and Medicine, Sendai, Japan;* [7]*Department of Hematology and Rheumatology, Department of Medicine, Tohoku University Graduate School of Medicine, Sendai, Japan; and* [8]*Department of Endocrinology and Hypertension, Tokyo Women's Medical University, Tokyo, Japan*

Submitted 15 April 2014; accepted in final form 3 December 2014

Narumi K, Hirose T, Sato E, Mori T, Kisu K, Ishikawa M, Totsune K, Ishii T, Ichihara A, Nguyen G, Sato H, Ito S. A functional (pro)renin receptor is expressed in human lymphocytes and monocytes. *Am J Physiol Renal Physiol* 308: F487–F499, 2015. First published December 10, 2014; doi:10.1152/ajprenal.00206.2014.— The renin-angiotensin system (RAS) is involved in inflammation. The signaling via the ANG II type 1 receptor in human lymphocytes and monocytes, which play key roles in pathophysiology of glomerulonephritis (GN), can enhance inflammation. However, the role of the (pro)renin receptor [(P)RR], a component of the RAS, in inflammatory reactions is unknown. We assessed whether (P)RR is expressed in human lymphocytes and monocytes by RT-PCR, Western blotting, flow cytometry, and immunohistochemistry, and whether (P)RR functions in inflammation. (P)RR mRNA and protein were expressed in human peripheral blood mononuclear cells (PBMCs). Flow cytometric analysis revealed high expression of (P)RR on monocytes. (P)RR was present on PBMCs, infiltrating lymphocytes, and macrophages around glomeruli with a crescent in anti-neutrophil cytoplasmic antibody (ANCA)-associated GN. Renin stimulation of PBMCs from healthy subjects in the presence of the ANG II type 1 receptor and ANG II type 2 receptor blockers induced ERK1/2 phosphorylation and release of IL-6 and expression of *cyclooxygenase-2 (COX-2)*. The increases in cytokine release and *COX-2* expression were inhibited in the presence of an ERK1/2 inhibitor. (P)RR knockdown by small interfering RNA in U937 cells, a human leukemic monocyte lymphoma cell line, significantly decreased ERK1/2 phosphorylation after renin stimulation. Thus (P)RR expressed in human inflammatory cells might contribute to inflammation in ANCA-associated GN.

(pro)renin receptor; renin-angiotensin system; lymphocytes; glomerulonephritis; human

INFLAMMATORY CELLS SUCH AS lymphocytes and macrophages infiltrate around the glomeruli and tubulointerstitial in glomerulonephritis (GN) and play a role in the progression of renal injury. Classically, B lymphocytes producing immunoglobulins (Ig) are involved in the pathogenesis of GN. T lymphocytes can abrogate inflammatory activity, leading to the amelioration of GN. In addition, macrophages have key functions in inflammation, tissue repair, and remodeling (30, 33). However, activation of these cells in the pathogenesis of GN is poorly understood.

The renin-angiotensin system (RAS) is essential for blood pressure control by regulating salt metabolism and body fluid volume. Angiotensin (ANG) II contributes to the pathophysiology of renal disease, cardiac hypertrophy (32), and atherosclerosis (47) by signaling through the ANG II type 1 receptor (AT_1R). AT_1R expressed by human B and T lymphocytes and monocytes (39) can enhance immune reactions (9). ANG II has significant proinflammatory actions in the vascular wall, including the production of reactive oxygen species, inflammatory cytokines, and adhesion molecules (7). Furthermore, the inhibition of the RAS is an effective treatment for autoimmune nephritis (17, 18). The therapeutic use of an angiotensin-converting enzyme (ACE) inhibitor reduced proteinuria and glomerular injury in a mouse model of lupus nephritis (18). However, the mechanism by which the RAS stimulates inflammatory cells is not fully understood.

The (pro)renin receptor [(P)RR], a specific receptor for renin and prorenin, is an important member of the RAS (36). When prorenin binds to (P)RR, it becomes the active form and produces ANG I from angiotensinogen. Although full-length and soluble forms of (P)RR have been isolated (10), the specific role of each is not known. In addition, (P)RR activation triggers MAPK ERK1/2 phosphorylation, which stimulates the production of transforming growth factor-β1 (TGF-β1) that mediates cell proliferation and fibrosis (35, 50). Thus (P)RR could act as an intracellular signaling receptor independently of ANG II and participate in the inflammatory reaction, including GN. However, there is no direct evidence that (P)RR is responsible for the activation of inflammatory cells involved in GN. Therefore, we hypothesized that (P)RR expressed in human lymphocytes and monocytes may participate in the activation of inflammatory cells and the progression of GN. To clarify this, we examined (P)RR expression in primary isolated human lymphocytes and monocytes and investigated ERK1/2 phosphorylation by renin stimulation using primary human lym-

* K. Narumi and T. Hirose contributed equally to this work.

Address for reprint requests and other correspondence: E. Sato, Div. of Nephrology, Endocrinology, and Vascular Medicine, Tohoku Univ. Graduate School of Medicine, 1-1 Seiryo-cho, Aoba-ku, Sendai 980-8574, Japan (e-mail: emiko@med.tohoku.ac.jp).

phocytes and monocytes and a human leukemic monocyte lymphoma cell line (U937). (P)RR is expressed by human lymphocytes and monocytes and is responsible for inflammation by activation of ERK1/2 via the renin-(P)RR pathway and inflammatory cytokine release. In addition, (P)RR was expressed by inflammatory cells present during active anti-neutrophil cytoplasmic antibody (ANCA)-associated GN.

MATERIALS AND METHODS

Human tissues and blood sampling. The study protocol was approved by the Institutional Review Board of the Tohoku University School of Medicine. All participants gave written informed consent after a full explanation of the purpose and potential risk involved in participating in the study.

Renal sections were obtained by renal biopsy of three patients diagnosed with ANCA-associated GN and three patients diagnosed with minimal-change nephrotic syndrome (MCNS). Venous blood was obtained from 12 healthy volunteers (6 men and 6 women, age range 21–45 yr). Plasma was collected concurrently to analyze biochemical parameters. Human brain tissues, pituitary glands, hearts, kidneys, and adrenal glands were obtained at autopsy for RT-PCR analysis and stored at −80°C until RNA extraction (43, 44). The tissues had no macroscopic pathological abnormalities.

Lymphocyte isolation. Peripheral blood mononuclear cells (PBMCs) were obtained as previously described (6). Briefly, PBMCs were prepared by layering whole blood on Ficoll-Paque PLUS (GE Healthcare, Uppsala, Sweden) and centrifuged at 300 *g* at room temperature for 20 min. The interphase of mononuclear leukocytes was carefully aspirated, washed two times in PBS (Sigma-Aldrich, Munich, Germany), and centrifuged at 1,500 rpm for 5 min. Cells were then resuspended in RPMI 1640 medium (Invitrogen, Carlsbad, CA) supplemented with penicillin G (100 IU/ml, Sigma-Aldrich) and streptomycin (100 μg/ml, Sigma-Aldrich). T cells, natural killer (NK) cells, and monocytes were separated from PBMCs by magnetically activated cell sorting (MACS).

Immunohistochemistry of (P)RR in human crescentic GN and PBMCs. Renal biopsies were fixed in 95% ethanol and paraffin embedded. Tissue blocks were cut into 1.5-μm sections for immunostaining and periodic acid-Schiff (PAS) staining. For immunostaining, paraffin sections were deparaffinized and incubated in methanol containing 0.3% H_2O_2 for 30 min and digested with collagenase to examine the effect of proteolytic or glycolytic enzymes on the reactivity of surface antigens. Cytospin slides were prepared from PBMCs after incubation with fixation buffer (00-8222-49, eBioscience, San Diego, CA) for 30 min. Both tissue and PBMCs slides were incubated in primary antibody overnight at 4°C in protein block serum-free solution (X0909, Dako, Glostrup, Denmark). Primary antibodies against lymphocytes were used as previously described (37). Antiserum against (P)RR was raised in a rabbit by injection of a human (P)RR fragment corresponding to 224–237 amino acids conjugated to BSA (19, 20). After washing, slides were incubated with Alexa Fluor 555 goat anti-rabbit antibody (A-21428, Life Technologies, Grand Island, NY) and Alexa Fluor 488 goat anti-mouse antibody (A-11001, Life Technologies) for 30 min in protein block serum-free solution. Then, slides were embedded in DAPI-Fluoromount-G (SouthernBiotech, Birmingham, AL) and observed by TCS-SP8 confocal microscopy (Leica, Wetzlar, Germany).

mRNA expression. Total RNA was extracted by Isogen (Nippon Gene, Toyama, Japan). Total RNA (4 μg) was reverse transcribed with 400 U of reverse transcriptase (PrimeScript; TaKaRa, Otsu, Japan) using an oligo (dT) primer, as previously described (19, 42).

PCR was performed in a total volume of 20 μl containing 80 ng of cDNA, 0.2 mmol/l of each deoxynucleotide triphosphate, 0.25 μmol/l of each primer, and 0.4 units of Taq DNA polymerase (Promega, Madison, WI). Primer sequences for *(P)RR* (GenBank accession no. NM005765) were as follows: sense (exon 8) 5′-CCTCCCTCATTAGGAAGACAAGGAC-3′, and anti-sense (exon 9) 5′-TCGAATCTTCTGGTTTGTCATCCT-3′. Expression of *GAPDH* mRNA was used as an internal control (40–42). After heating at 94°C for 2 min, denaturation, annealing and elongation were carried out at 94°C for 15 s, 64°C for 30 s, and 72°C for 1 min, respectively, and the reactions were repeated for 25 cycles, followed by incubation at 72°C for 5 min.

(P)RR expression in lymphocytes and monocytes and *cyclooxygenase-2* (*COX-2*) in PBMCs were quantified by real-time PCR. Five nanograms of cDNA was amplified in duplicate using SYBER Premix Ex Taq II (TaKaRa Bio) on CFX96 (Bio-Rad). The same primers of *(P)RR* as above were used. Primers of *COX-2* (HA143872) and *GAPDH* (HA067812) were purchased from TaKaRa Bio. After heating at 95°C for 2 min, denaturation, annealing and elongation were carried out at 95°C for 5 s and 60°C for 20 s, respectively, and the reactions were repeated for 39 cycles, followed by incubation at 65°C for 5 s.

Western blot analysis. PBMCs were collected by centrifuging at 1,500 rpm for 10 min and resuspended with RIPA buffer (Cell Signaling Technology, Danvers, MA) containing a protease inhibitor (Roche, Basel, Switzerland), Laemmli Sample Buffer (161-0737, Bio-Rad, Hercules, CA), and β-mercaptoethanol (Bio-Rad). U937 cells were lysed with RIPA buffer (Cell Signaling Technology) containing a protease inhibitor (Roche) and phosphatase inhibitor (Sigma-Aldrich) after renin stimulation. After boiling at 95°C for 5 min, protein extracts were separated by 12% SDS-PAGE for 90 min at 150 V and transferred electrophoretically to polyvinylidene difluoride membranes (Bio-Rad) for 1 h at 100 V, 4°C. Membranes were incubated in TBS (10 mmol/l Tris·HCl, 150 mmol/l NaCl) with 5% nonfat dry milk or 10% BSA for 1 h, then incubated with primary antibody [anti-(P)RR, 1:5,000; anti-ERK, 1:1,000, 4695S, Cell Signaling; anti-p-ERK, 1:1,000, 4377S, Cell Signaling Technology] overnight at 4°C in TBS with 2% nonfat dry milk or 5% BSA. Membranes were washed three times in TBS with 0.08% Tween 20 for a total of 30 min and incubated with horseradish peroxidase (HRP)-conjugated secondary antibody (anti-rabbit IgG, 1:5,000, sc-2,004; anti-mouse IgG, 1:5,000, sc-2005; Santa Cruz Biotechnology, Santa Cruz, CA) for 1 h in TBS with 2% nonfat dry milk or 5% BSA. After washing three times in TBS with 0.08% Tween 20, chemiluminescence (ECL Western blotting detection system; Amersham, Arlington Heights, IL) was measured using VersaDocMP5000 (Bio-Rad). Expression of β-actin (1:5,000, sc-47778, Santa Cruz Biotechnology) was used as an internal control. Specificity of the antiserum against (P)RR was examined using an absorption test, performed using antiserum incubated with an excess amount of human $(P)RR_{224-237}$ (10 nmol) for 20 h at 4°C prior use.

Flow cytometric analysis. Six-color flow cytometric analyses were performed on a FACS Canto II, with a FACS Aria II (Becton Dickinson, Franklin Lakes, NJ) for cell sorting. Within 30 min after cell isolation, PBMCs (3×10^5 cells) were stained for 30 min on ice using the corresponding antibodies and washed three times with PBS after blocking with goat IgG to avoid reactivity to the secondary antibody. Three samples used different antibody combinations for staining as follows: *1*) anti-(P)RR antibody-PE, anti-CCR7-FITC, anti-CD4-PerCP, anti-CD45RA-APC, anti-CD3-V450, anti-CD8-APC-Cy7 or anti-(P)RR antibody-PE, anti-CD19-PerCP, and anti-CD56-Pacific blue; *2*) nonimmune rabbit serum and anti-CD antibodies as above; and *3*) nonimmune rabbit serum and isotype control. Monocytes were analyzed by gating on the monocyte population assessed by forward- and side-scatter dot plots. Data were analyzed by FlowJo software (Tree Star, Ashland, OR). After immunostaining, cells were resuspended in PBS and analyzed immediately by flow cytometry with DIVA software (Becton Dickinson). The cutoff value of fluorescence was 99% negative for the control.

To analyze (P)RR expression on lymphocytes and monocytes, isolated PBMCs were incubated with an anti-(P)RR antibody, followed by a PE-conjugated secondary goat-anti-rabbit antibody (1:100,

20303, Imgenex, San Diego, CA) for 30 min on ice at each step. Serum obtained from the rabbit before immunization with the peptide fragment (nonimmune rabbit serum) was used as a respective isotype control for the anti-(P)RR antibody.

After renin stimulation, cells were fixed in fixation buffer (00-8222-49, eBioscience) for 20 min at room temperature and washed two times with permeabilization buffer (00-8333-56, eBioscience). Then, cells were stained for 1 h at room temperature using phospho-ERK (p-ERK) antibody, followed by PE-conjugated secondary goat-anti-rabbit antibody (1:100, 20303, Imgenex) for 30 min at room temperature.

ERK1/2 phosphorylation by renin stimulation. To prevent signaling through AT_1R and the ANG II type 2 receptor (AT_2R), isolated PBMCs were preincubated in RPMI 1640 containing penicillin G (100 IU/ml), streptomycin (100 μg/ml), AT_1R blocker losartan (10 μmol/l), and AT_2R blocker PD123319 (10 μmol/l) for 60 min. To examine whether renin stimulation induces cytokine releasing through the ERK1/2 pathway, a specific ERK1/2 inhibitor, U0126 (10 μmol/l, U120, Sigma-Aldrich), was incubated with RPMI 1640, penicillin G (100 IU/ml), streptomycin (100 μg/ml), AT_1R blocker losartan (10 μmol/l), and AT_2R blocker PD123319 (10 μmol/l) for 60 min. Thereafter, cells were incubated in medium containing human recombinant renin (2 or 20 nmol/l, R2779, Sigma-Aldrich) for 0, 6, and 24 h. We used 50 mmol/l Tris·HCl buffer as a vehicle control.

Measurement of renin-induced cytokine release by cytometric bead array. Release of cytokines (IL-2, IL-4, IL-6, IL-10, IFN-γ, and TNF-α) released from lymphocytes and monocytes were measured by a BD Human Th1/Th2 Cytokine cytometric bead array kit II (Becton-Dickinson) according to the manufacturer's instructions. Fifty microliters of supernatant was stained with a suspension containing a mixture of human cytokine capture beads and a PE detection reagent. After 3 h of incubation, samples were washed and analyzed. Standards provided with the kit were appropriately diluted and used in parallel for preparation of the standard curves.

Cell culture and small interfering RNA transfection. U937 cells (American Type Culture Collection CRL-1593.2) were cultured in RPMI 1640 supplemented with 10% FBS (Life Technologies), penicillin G (100 IU/ml), streptomycin (100 μg/ml), and pyruvate acid (100 mmol/l) at 37°C in humidified air with 5% CO_2. Medium was changed every 3 days. Cells were serum starved for 24 h before the renin stimulation experiments were performed. (P)RR small interfering RNA (siRNA; LQ-013647-01-0005, Thermo Scientific) or non-targeting control siRNA (D-001810-10-05, Thermo Scientific) were transfected into U937 cells by electroporation (4D-Nucleofector,

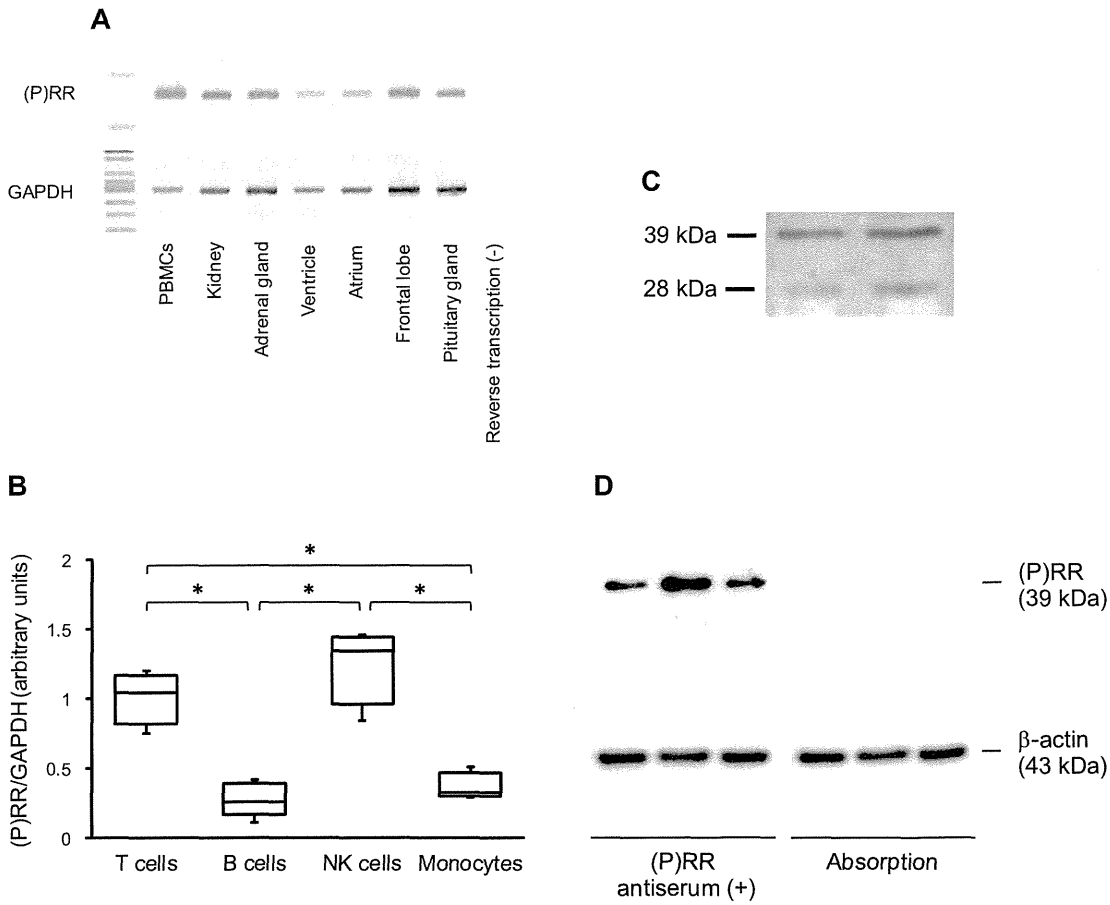

Fig. 1. Expression of (pro)renin receptor [(P)RR]. *A*: expression of *(P)RR* mRNA in human peripheral blood mononuclear cells (PBMCs), kidney, adrenal gland, heart, frontal lobe, and pituitary gland. Reverse transcription (−; samples without RTase treatment) indicates negative controls ($n = 2$). *Glyceraldehyde-3-phosphate dehydrogenase* (*GAPDH*) was used as an internal control. *B*: *(P)RR* mRNA in subpopulations of lymphocytes and monocytes by real-time PCR ($n = 12$). Values are presented as the median (central line), interquartile range (box), and range (whiskers). *$P < 0.05$. *C*: expression of (P)RR protein in human PBMCs ($n = 2$) by Western blot analysis. Both full-length (39 kDa) and soluble form (28 kDa) of (P)RR were expressed in PBMCs. *D*: expression of (P)RR protein in human PBMCs ($n = 3$) by Western blot analysis. (P)RR antiserum (+), PBMC samples treated with antiserum against (P)RR; Absorption, PBMC samples treated with antiserum against (P)RR preabsorbed with synthetic human $(P)RR_{224-237}$. (P)RR gave a strong signal with a molecular weight of 39 kDa. As an internal control, the membranes were rehybridized with β-actin antibody.

Lonza, Switzerland). To assess the effect of (P)RR knockdown in cell growth or viability, a 3-(4,5-dimethylthiazol-2yl)-2,5-diphenyltetrazolium bromide (MTT) assay (10009365, Cayman Chemical) was performed according to the manufacturer's protocol.

Statistical analysis. Continuous values were given as the median and interquartile range. Statistical comparisons were made using a Mann-Whitney *U*-test for two-group comparison and the Kruskal-Wallis test, followed by a Mann-Whitney *U*-test for multiple comparisons of differences among the groups. Statistical significance was considered when $P < 0.05$.

RESULTS

(P)RR mRNA and protein expression. (P)RR mRNA was expressed in all tissues tested and PBMCs (Fig. 1*A*). We also investigated the expression of (P)RR mRNA in T, B, NK cells, and monocytes after isolating PBMCs by flow cytometer sorting. (P)RR mRNA was highly expressed in T cells and NK cells (Fig. 1*B*). A 39-kDa band corresponding to full-length (P)RR protein was clearly detected by Western blotting. Furthermore, we detected a very weak 28-kDa band corresponding to the soluble form of (P)RR protein (Fig. 1*C*). Bands from (P)RR protein but not β-actin were abolished by preabsorption with human $(P)RR_{224-237}$ peptide (Fig. 1*D*).

(P)RR expression in human lymphocytes and monocytes. Positive (P)RR staining was observed in T cells ($CD3^+$, Fig. 2*A*), B cells ($CD22^+$, Fig. 2*B*), NK cells ($CD56^+$, Fig. 2*C*), and monocytes ($CD68^+$, Fig. 2*D*). Localization of fluorescent sig-

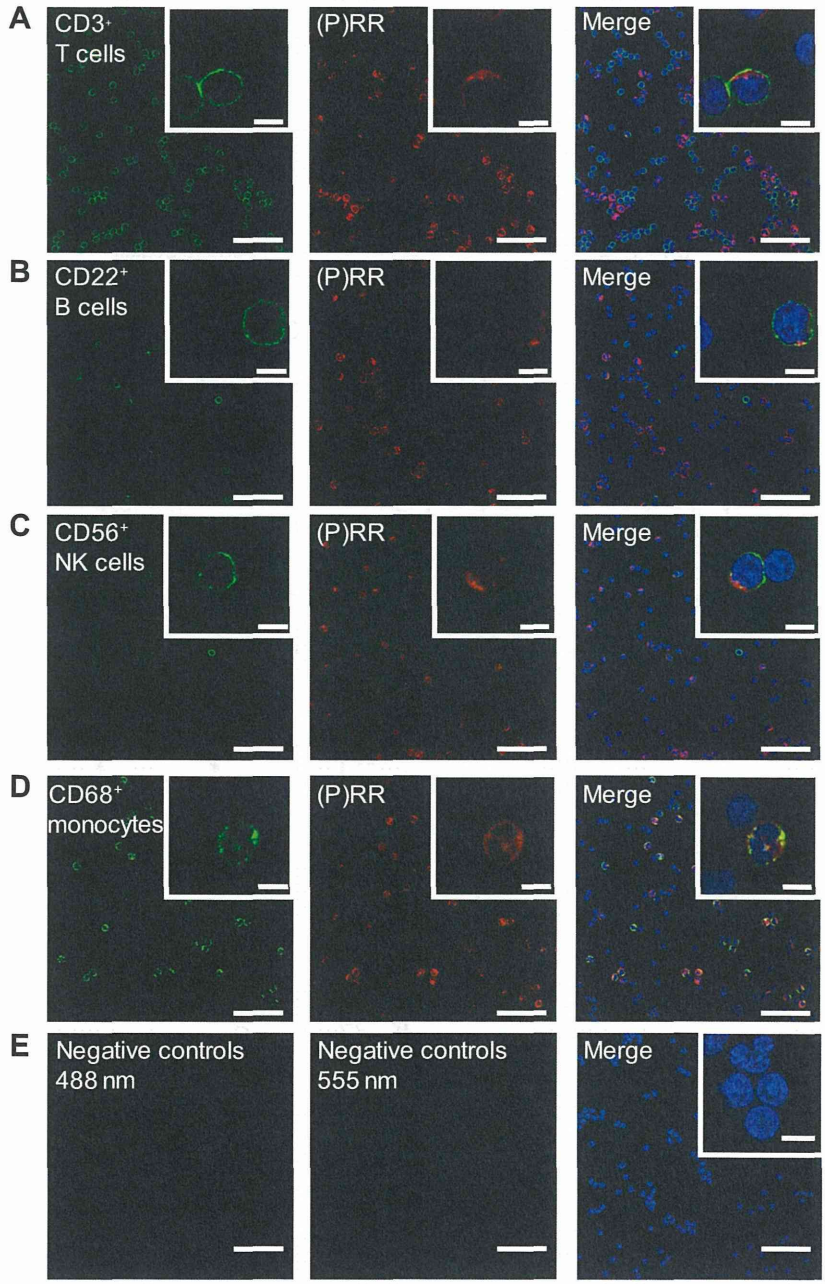

Fig. 2. Immunohistochemical study of (P)RR in human PBMCs. *Left*: lymphocytes or monocytes stained with specific antibodies (green). *A*: $CD3^+$ T cells. *B*: $CD22^+$ B cells. *C*: $CD56^+$ natural killer (NK) cells. *D*: $CD68^+$ monocytes. *E*: negative controls. *Middle*: $(P)RR^+$ lymphocytes or monocytes stained with (P)RR-specific antibodies (red). *Right*: merged pictures and nuclear stain with 4,5-diamidino-2-phenylindole (DAPI). Scale bars of low-power field = 5 μm and that of high-power field = 50 μm.

nals suggested (P)RR might be expressed within the cell cytosol rather than on the cell surface except $CD68^+$ monocytes. In $CD68^+$ monocytes, the immune signals of (P)RR are overlapping with that of CD68. Isotype sera showed no positive immunofluorescence (Fig. 2*E*).

(P)RR expression in human lymphocytes by flow cytometric analysis. Discrimination between targeted cells (lymphocytes and monocytes) and other cells (granular leukocytes and red blood cells) was achieved by forward and side scatter. PBMCs treated with anti-(P)RR antibodies showed (P)RR positivity compared with those treated with nonimmune rabbit serum (Fig. 3, *A* and *B*). Samples treated with anti-(P)RR antibodies showed (P)RR positivity compared with those treated with nonimmune rabbit serum or isotype control (Fig. 3*C*). Figure 3*D* shows a dot plot of (P)RR-positive cell rate from lymphocyte subsets and monocytes of 12 healthy subjects. The ex-

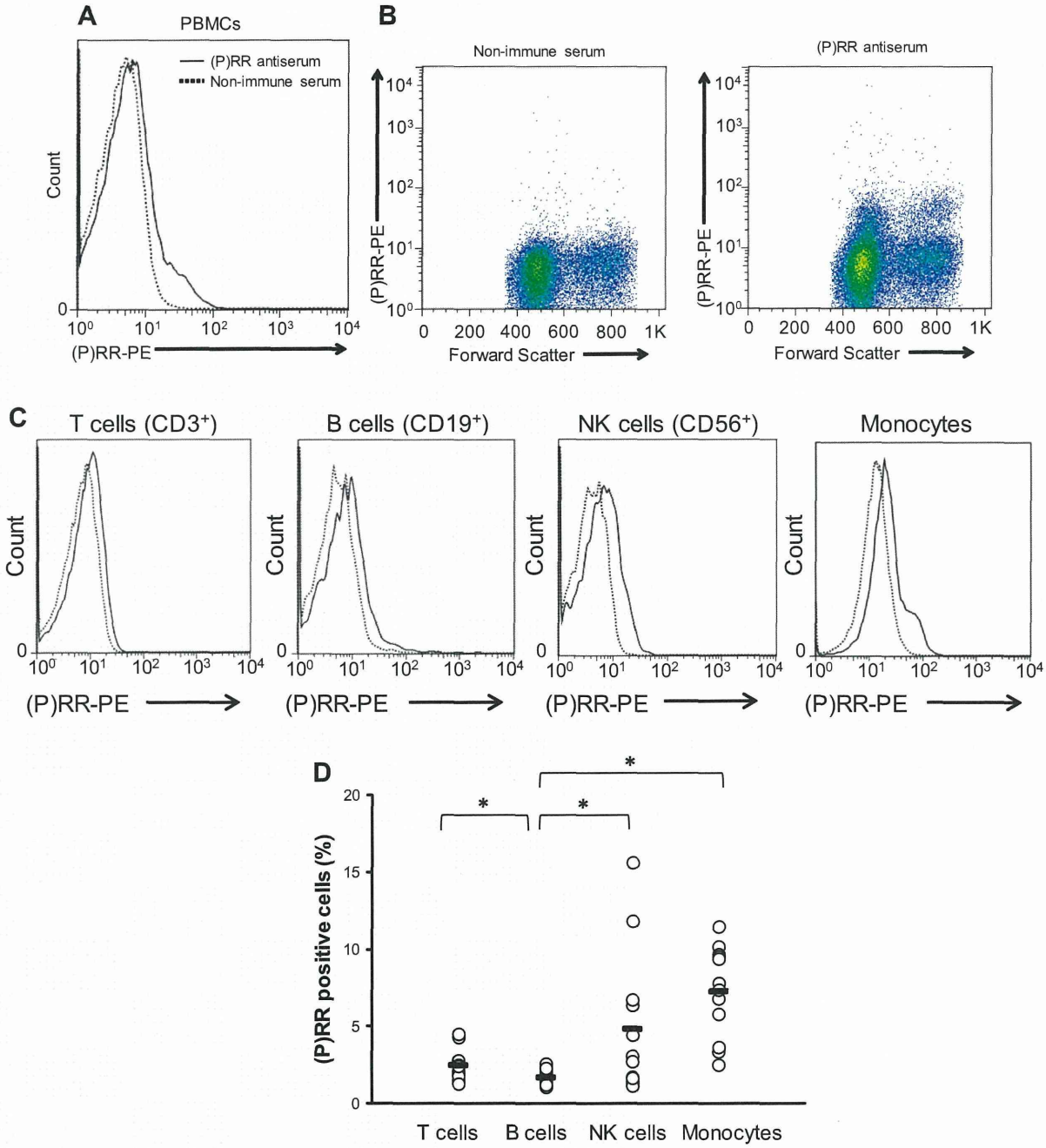

Fig. 3. Flow cytometric analysis of (P)RR protein in human PBMCs. *A*: representative flow cytometry histogram of PBMCs treated with (P)RR antiserum (solid line) or nonimmune serum (dotted line). *B*: representative flow cytometry dot plots of PBMCs treated with (P)RR antiserum (*right*) or nonimmune serum (*left*). *C*: representative histograms of (P)RR-PE expression by $CD3^+$ T cells, $CD19^+$ B cells, $CD56^+$ NK cells, and monocytes. Solid line, treated with (P)RR antiserum; dotted line, treated with nonimmune serum. *D*: dot plot representing (P)RR-positive subpopulations ($n = 12$). Bold lines represent mean. $^*P < 0.05$ compared with B cells.

pression level of (P)RR in monocytes, NK cells, and T cells was significantly higher than for B cells ($P < 0.05$). (P)RR expression tended to be high in monocytes compared with other cell types.

Renin-induced ERK phosphorylation and cytokine production. To investigate whether (P)RR in human lymphocytes and monocytes is functional, we focused on renin-induced ERK1/2 signaling. Human recombinant renin induction of ERK1/2 phosphorylation was renin concentration and time dependent (Fig. 4, *A* and *B*). In this study, we used 20 nmol/l renin after stimulation experiments. Figure 4*C* shows a box plot of the ERK1/2 phosphorylation-positive cell rate before renin stimulation (prestimulated) and after stimulation (poststimulated) of PBMCs from nine healthy subjects. P-ERK-positive cells were significantly increased by renin stimulation ($P < 0.01$). Moreover, after isolation of each cell type (T cells, NK cells, and monocytes) from three volunteers, we analyzed renin-induced ERK1/2 phosphorylation. In respective cells, the histograms shifted to the right, suggesting ERK1/2 phosphorylation was induced by renin (Fig. 4*D*). We could not investigate B cells because of low cell numbers in total lymphocytes.

We also examined whether cytokines were released after renin stimulation of PBMCs from six healthy subjects. Figure 5*A* indicates dot plots of each cytokine tested. The *left* and *right* panels show prestimulated (0 h) and poststimulated (after 24 h) levels, respectively. The release of IL-6, IL-10, and IFN-γ was renin concentration and time dependent (Fig. 5*B*). Furthermore, to determine which cells reacted to renin, we examined cytokine release after isolation of T, B, NK cells, and monocytes from PBMCs ($n = 6$) by flow cytometer. IL-6 was mainly secreted by monocytes (Fig. 5*C*).

To examine the effect of the ERK1/2 pathway on cytokine secretion, we performed the experiments using the ERK1/2 inhibitor U0126. We focused on IL-6 because this concentration was higher than the other cytokines after renin stimulation. Figure 6 indicates box plots of the change in each cytokine releasing with or without U0126 after stimulation of renin or Tris·HCl as a vehicle control. IL-6 in response to renin was significantly increased, and IL-6 was attenuated under U0126.

COX-2 expression. *COX-2* is considered to be an important enzyme for the inflammatory reaction including the ERK1/2 pathway. To identify *COX-2* expression via the ERK1/2 pathway after renin stimulation, we performed the experiments

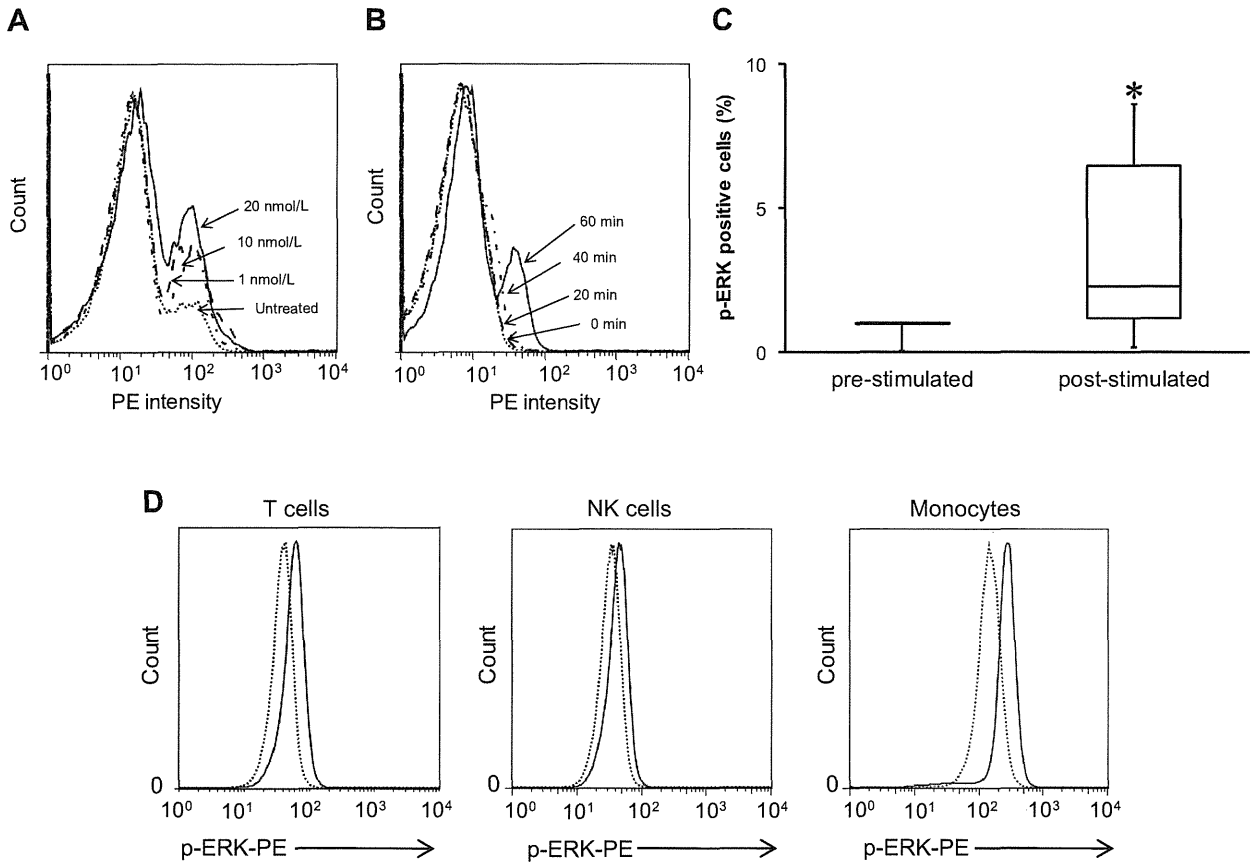

Fig. 4. Flow cytometric analysis of ERK1/2 phosphorylation-positive cells induced by renin in primary human PBMCs. *A*: representative histogram of phospho-ERK1/2 (p-ERK)-positive cells after incubation with 0 nmol/l (untreated) and 1, 10, and 20 nmol/l renin. Dotted line, untreated; dashed line, 1 nmol/l; complex line, 10 nmol/l; solid line, 20 nmol/l. *B*: representative histogram of p-ERK-positive cells 0, 20, 40, and 60 min after 20 nmol/l renin stimulation. Dotted line, prestimulated; dashed line, 20 min; complex line, 40 min; solid line, 60 min. *C*: box plots representing the percentage of p-ERK-positive cells from total PBMCs ($n = 9$). Values are presented as the median (central line), interquartile range (box), and range (whiskers). *$P < 0.05$ compared with prestimulated. *D*: representative examples of flow cytometry histograms of p-ERK of T cells, NK cells, and monocytes. Solid line, treated with (P)RR antiserum; dotted line, treated with nonimmune serum.